DIFFERENTIAL PROTEOMIC ANALYSIS OF THE MOUSE RETINA : THE INDUCTION OF CRYSTALLIN PROTEINS BY RETINAL DEGENERATION IN THE *rd*1 MOUSE

Nükhet Cavusoglu[1†] , Danièle Thierse[2], Saddek Mohand-Saïd[2], Frédéric Chalmel[3],

Olivier Poch[3], Alain Van-Dorsselaer[1], José-Alain Sahel[2], Thierry Léveillard[2‡]

Address :

1 Laboratoire de Spectrométrie de Masse Bio-Organique, CNRS UMR 7509, ECPM, 25 rue Becquerel, 67087 Strasbourg cedex- France.

2 Laboratoire de Physiopathologie moléculaire et cellulaire de la rétine, INSERM U592, Hôpital St-Antoine, 184 rue du Faubourg St-Antoine, 75571, Paris cedex 12-France

3 Institut de Génétique et de Biologie Moléculaire et Cellulaire, 1 rue Laurent Fries, 67404 Illkirch-France

† Present address : Laboratoire de Physiopathologie moléculaire et cellulaire de la rétine, INSERM U592, Hôpital St-Antoine, 184 rue du Faubourg St-Antoine, 75571, Paris cedex 12-France

‡ Corresponding author : Thierry Léveillard, Ph : (0)1 49 28 46 03 ; FAX : (0)1 49 28 46 05

leveilla@st-antoine.inserm.fr

Running title : Proteomic of the *rd1* mouse

Summary :

We have applied proteomic analysis to the degeneration of photoreceptors (PR). In the *rd1* mouse a recessive mutation in the PDE6B gene leads to rapid loss of rods through apoptosis. By five weeks postnatal, virtually all rod PR have degenerated leaving one row of cones that degenerates secondarily. In order to assess comparative protein expression, proteins extracted from whole retina were resolved on a 2D gel and identified by mass spectrometry combined with database screening. MALDI-TOF mass spectrometry coupled to peptide mass fingerprinting was sufficient to identify most of the proteins, the remaining being identified with additional sequence information obtained by nanoESI-MS/MS or LC-MS/MS. The study revealed 212 spots, grouped into 109 different proteins. Differential analysis showed loss of proteins involved in the rod-specific phototransduction cascade as well as induction of proteins from the crystallin family, in response to retinal degeneration. Identification of such pathways may contribute to new therapeutic approaches.

Introduction :

The *rd1* mouse carries a recessive mutation in the gene coding for the beta subunit of cGMP-phosphodiesterase (PDE6B) selectively expressed by rod photoreceptors (PR) and is a widely used model of inherited retinal degeneration (1). The defect in rod phosphodiesterase activity and consequent rise in intracellular cGMP concentration (2) lead to rapid loss of rods through apoptosis (3-4). By five weeks postnatal, virtually all rods have degenerated leaving one row of cones that undergo secondary degeneration (5). Experimental evidence suggests that secondary cone degeneration in this model results from loss of trophic support mediated by protein(s) secreted in the presence of rods (6-7). Differential analysis would permit identification of proteins whose expression is lost following rod degeneration, and potentially those mediating cone viability. Analysis of gene expression in this model has already led to discovery of genes essential for photoreceptor function that are often found to be mutated and cause retinal degeneration in humans (8-9). These analyses have measured the steady state levels of mRNA using DNA chips (10-11) and SAGE (12). It has been observed that mRNA levels are not directly correlated to protein expression (13). Because biological functions are performed by proteins, we conducted differential analysis of *rd1* versus wild type mouse retina at the protein level. In order to display retinal proteins, we separated retinal extracts by 2D gel electrophoresis and identified stained protein spots by mass spectrometry followed by database searching. All the spots were first analysed by MALDI-TOF mass spectrometry, the generated data being used to perform matching. This approach by peptide mass fingerprinting described in the early 90s permitted identification of >90% of the analysed spots (14-17). For the remaining spots that could not be resolved by this approach, we used tandem mass spectrometry with direct injection by nano-ESI-MS/MS (18-20) or after an additional separation step, by nano-LC MS/MS (21).

This study provides an analysis of the most abundant soluble proteins expressed in the adult mouse neural retina. In addition, comparison with *rd1* retina after rods have degenerated demonstrates elevated expression of proteins of the crystallin family, indicating a possible endogenous mechanism of neuroprotection.

Experimental procedures :

Animals

Care and handling of mice in these studies conformed to the Association for Research an Vision and Ophthalmology Resolution on the use of animals in research. C3H/HeN mice homozygous for the retinal degeneration 1 gene (*rd1*), and C57Bl/6 normal sighted mice, were obtained from Iffa-Credo Animal Suppliers (France).

Tissue extraction and 2D gel electrophoresis

All chemicals when not specified were from Sigma (St Louis, MO) and for DTT and iodoacetamide from Fluka (Buchs, Switzerland).

Neural retinas were dissected in phosphate buffer saline (PBS), and immediately transferred to extraction buffer : Tris 50 mM pH 7.5 ; PMSF 1 mM ; EDTA 1 mM ; DTT 1 mM, protease inhibitors cocktail (Complete from Roche, Basel, Switzerland) for 45 minutes at 4°C. After a few seconds of sonication, the concentration of each extract was determined by Bradford assay. 500 µg of extracted protein were evaporated and suspended in rehydration buffer : 7 M urea ; 2 M Thiourea ; 4 % Chaps ; 0.24 % Triton X100 ; 20 mM DTT ; 20 mM spermine ; 0.6% ; Biolyte pH range 3-10 (Biorad, Hercules, CA). The samples were incubated 30 min at 20°C and centrifuged 30 min at 15.000 rpm at 20°C. Protein extracts were loaded strips of pH range 3-10 (Biorad) during 15 hours at 20°C under 50 V in a PROTEAN IEF cell (Biorad). The isoelectric focusing was performed by steps of increased voltage : 1 hour at 150, 300, 600 and 1000 V followed by 15 hours at 3000 V and finally 6 hours at 500 V at 20°C. The

strips were incubated 30 min at 20°C in electrophoresis buffer : 50 mM Tris-HCl pH 8.8 ; 6 M urea ; 30 % (v/v) Glycerol ; 2% (w/v) SDS and 65 mM DTT and followed by 30 min in the same buffer containing 26 mM iodacetamide. The second dimension was performed in a gradient gel (5-15% acrylamide) on a PROTEAN II (Biorad) at 5 mA/gel for 3 hours and 10 mA/gel overnight. The gels were stained by coomassie brilliant blue (R 250, Sigma, St Louis, MO), spots were selected by visual inspection and gel slices were excised by scalpel.

Western blotting

For western blotting, 40 µg of protein from 2 and 5-weeks old C57BL/6 and C3H/He neural retina extracts were loaded on a 10% SDS-PAGE then transferred onto nitrocellulose membrane (Optitran, Schleicher & Schuell, Dassel, Germany). The nitrocellose membrane was saturated over night at 4°C with blocking solution [3% Non dry fat milk (Blocker, Biorad) and 0.1% Tween-20 (Sigma) in PBS]. The polyclonal anti α-crystallin B (Chemicon, Temecula, CA) was incubated during 3 hours at room temperature at a dilution of 1/5,000 in blocking solution then washed 4 times in PBS 0.1% tween-20, then incubated one hour at room temperature with goat anti-rabbit coupled to peroxydase (Jackson ImmunoResearch Laboratories, West Grove, PA) at a dilution of 1/15,000 in blocking solution. The nitrocellulose membrane was extensively washed 4 times in PBS 0.1% tween-20, then the chemoluminescent reagents were added (ECL plus, Amersham Biosciences, Buckingham, UK) and antibodies revealed by autoradiography on Biomax light film (Kodak, Rochester, NY). For standardisation, a gel was loaded with the same extracts and probed with the monoclonal anti-α-tubulin (Sigma) at a dilution of 1/500 and revealed with an goat anti-mouse at 1/15,000 following the same procedure.

In gel digestion procedure

Each gel slice was cut into small pieces with a scalpel, washed with 100 µl of 25 mM NH_4HCO_3 (Sigma), and then with 100 µl of acetonitrile, as already described (22). After the

washing step, gel pieces were completely dried with a Speed Vaccum for the reduction-alkylation step as described. The supernatant was removed and the washing procedure with 100 µl of NH_4HCO_3 and acetonitrile was repeated three times. Finally, gel pieces were again completely dried before tryptic digestion and swelled in a solution of trypsin (12.5 ng/µl, Promega, Madison, MA, USA) in 25 mM NH_4HCO_3. The digestion was performed at 35°C overnight, and the extraction step was performed with H_2O/5% HCOOH. The mixture was sonicated 10 min. and left a minimum of one hour at room temperature, permitting passive elution of the peptides.

MALDI-TOF Mass Spectrometry

Mass measurements were carried out on a BIFLEX III™ Matrix-Assisted Laser Desorption Ionisation Time-Of-Flight Mass Spectrometer (Bruker, Bremen, Germany) equipped with the SCOUT™ High Resolution Optics with X-Y multi-sample probe and griddles reflector. This instrument was used at a maximum accelerating potential of 19 kV and was operated in reflector mode. Ionisation was accomplished with a 337 nm beam from a nitrogen laser with a repetition rate of 3 Hz. The output signal from the detector was digitised at a sampling rate of 2 GHz. A saturated solution of α–cyano-*4*-hydroxycinnamic acid in acetone was used as matrix. A first layer of fine matrix crystals was obtained by spreading and fast evaporation of 0.5 µl of matrix solution. On this fine layer of crystals, a droplet of 0.5 µl of aqueous HCOOH (5%) solution was deposited. Afterwards, 0.5 µl of sample solution was added and a second droplet 0.2 µl of matrix saturated solution in 50% H_2O/50% ACN was added. The preparation was dried under vacuum. Prior to deposit samples were concentrated between 5 and 10 fold on zip-tip_{c18} (Millipore). The sample was washed once to three times by applying 1µl of aqueous HCOOH (5 %) solution on the target and then flushed after a few seconds. The calibration was performed in internal mode with 4 peptides, angiotensine, substance P,

bombesin and trypsin autolysis fragments with mono-isotopic $(M+H)^+$ at *m/z* 1046.542, 1347.736, 1620.807 and 2211.107 respectively.

nanoLC tandem Mass Spectrometry

Experiments were performed on extracted tryptic peptides from 2D gels. High Pressure Liquid Chromatography separation was performed on a CapLC ™ system (Waters, Milford, MA, USA). The system was coupled via a nanoLC inlet to the Q-TOF mass spectrometer (Micromass Ldt., Altricham, U.K) equipped with a nano-electrospray (Z-spray) source. Peptides were first desalted and then concentrated on a reverse phase pre-column of 300 µm ID (µprecolumn™, LC Packings, San Francisco, CA, USA), by solvent C (H_2O/ 0.1% HCOOH) delivered by an independent pump at a flow rate of 30 µl/min. The gradient was formed by the activation of two complementary pumps A and B, delivering respectively solvent A (H_2O/ 0.1% HCOOH) and solvent B (ACN/ 0.1% HCOOH) at a flow rate of 3 µl/min. A split of 1/10 allowed the flow rate to be decreased to 300 nl/min. Peptides were eluted through a reverse phase capillary column of 75 µm ID (PepMap, C18, LC Packings,) with a linear gradient from 5 to 95% of solvent B over 60 min under the control of the MassLynx 3.5 software. The eluted peptides were analysed by tandem mass spectrometry with an automated MS-to-MS/MS switching protocol when doubly or triply charged ions (precursor ions) were detected up to 10 counts/sec over the *m/z* range 200 to 2000. In the MS experiment, precursor ions were measured in positive detection mode with a cone voltage of 30 V and selected by the quadrupole. The collision-induced dissociation MS/MS process was performed with collision energy between 20-50 eV in the collision cell and argon as the collision gas. The multimode analysis capacity of the Q-TOF II, permitted the analysis of co-eluted peptides with the ability to perform MS/MS experiments on 8 different ions (8 different channels) in parallel. MS/MS spectra containing fragment ions in multiple charge

states were deconvoluted using MaxEnt-3 software into single charged and mono-isotopic ion spectra.

Database search

Ions obtained from MALDI spectra were directly used for database searches using the software MS-Fit developed at the UCSF Mass spectrometry facility and available on the internet to search against protein databases (SWISS-PROT and NCBI). Database searches were performed using the following values, protein molecular weight range of 10-200 kDa, trypsin digest with one missing cleavage allowed, cysteines modified by carbamidomethylation, possible oxidation of methionines and mass tolerance of 50 ppm. The identification was based upon at least four matching peptides. The percentage of protein coverage (with peptides measured with 50 ppm mass tolerance) was taken into account for validation of protein identification.

Data resulted from LC-MS/MS were converted into a peak list containing all mono-isotopic peaks and submitted to the SWISS-PROT database via Global Server 1.0 search engine (Micromass, Manchester, U.K.). The peptide mass was set to 0.5 Da and the MS/MS tolerance to 0.25 Da. The MS/MS analysis results were search by BLAST after manual interpretation of spectra. Gene identities were extracted using specifically designed algorithms.

Results :

We performed 2D gel electrophoresis with whole cell extracts of wild type retina. The left panel of figure 1 illustrates the profile obtained with wild type retina after coomassie staining. Coomassie blue was selected in preference to silver stain for reasons of compatibility with mass spectrometry, despite the better sensitivity of silver stain (23). The right panel of figure 1 shows that the profile obtained with 5 week *rd1* mouse retina is similar to that of wild type

in many respects, with only a few spots missing from rodless retina, and parallel expression of new proteins induced by rod degeneration. To directly visualise PR-specific proteins, gel analysis of the outer nuclear layer, which contains uniquely PR cell bodies was performed (Fig. 2). This fraction was isolated by vibratome sectioning of flat-mounted retina from wild-type 5 week old mice (24). The protein spots were excised, washed and digested with trypsin. The mass of the resulting peptides were measured using MALDI mass spectrometry. In Table 1 representing the list of proteins identified, the entries annotated A(n) correspond to spots from analysis of wild type total retina; the B series represents proteins identified from *rd1* mouse total retina; and the C series is the list of proteins identified from the PR layer of wild type retina. The relevance of these identifications is essentially based on the number of matching peptides combined with the high mass accuracy of the measure. Even if 4 matching peptides and 50 ppm mass tolerance for database searches were required, the average peptide mass accuracy of identified proteins in Table 1 is 15 ppm (+/-5), and the number of matching peptides, expressed as % protein sequence coverage, always represents >4 peptides. These two criteria are reliable and allowed the unambiguous identification of the listed proteins (19).

Despite the limited resolution of 2D gel electrophoresis, through the use of MALDI-TOF MS it was possible to detect multiple proteins in the same spot. For multiple identifications, peptide masses assigned for the protein identified with the highest coverage were excluded, and the remaining list of masses was used to search the database (25). An example of the complexity of the mass spectrum obtained is shown in figure 3, where more than 100 peptides have been measured with mono-isotopic resolution. This analysis permitted the identification of four different proteins, phosphoglycerate mutase (PgM), phosphoglycerate kinase (PhK), creatine kinase (CKm) and pyruvate kinase (PyK). These proteins of very similar molecular weight (MW) from 44.5 to 57.9 kDa are not resolved on

the gel, even if their pI show a variation over 1.5 pH unit that should theoretically permit their separation. Post-translational modifications can induce variations in their pI and thus interfere with separation. These post-translational modifications also led to multiple spots for the same protein, for example glutamine synthase (GIS), lactate dehydrogenase (LDH) and pyruvate kinase (PyK) (26). This phenomenon could also result from an incomplete isoelectric focusing (27).

In cases where MALDI-TOF analysis did not reach the criteria cited above, tandem mass spectrometry was used to obtain sequence information and used in data mining. This additional procedure allowed unambiguous identification of proteins. In some cases, high abundance contaminant peptides (trypsin autolysis fragments, keratin contaminants) can suppress the detection of peptides of interest using the MALDI-MS approach (28). In order to detect these peptides, liquid chromatography coupled with tandem mass spectrometry (LC-MS/MS) was performed. The chromatographic step (nanoLC) prior to MS analysis permitted fractionation of the peptide mixture prior to spectrometric analysis. Thus each peak characterized by its mass over charge ratio (*m/z*) is further analysed by collision-induced dissociation (CID) MS/MS (29). It is clear that MALDI and nano-electrospray (nano-ESI) ionisation modes were very complementary, and the use of two different ionisation processes contributed to detection of a wider range of peptides (30). In figure 4, three examples of MS/MS spectra are presented. Panel a and b represent MS/MS spectra obtained after CID experiments on doubly charged ions at *m/z* 513.35 and *m/z* 488.32, which both led to the identification of an unique protein, the elongation factor EF1α (Eα1). The interpretations of the spectra after deconvolution with MAXENT 3 (Masslynx 3.5 software, Micromass) conducted on y series ions (classification according to reference (31)) led to the interpretation of the amino-acid sequences [GIGTV(PV)GR and PLQDVYK] shown in figure 4 and Table 2. These peptides covered 6% of the protein sequence. With regard to the MS/MS spectrum

in figure 4c, a unique sequence [SPI/LVVI/LSKGK] allowed unambiguous identification of the protein Ulip2. Independently of the search engine used to interrogate the database, use of either the interpreted sequence or the generated peak list led to unambiguous identification of Ulip2 protein. Table 2 gives the list of additional proteins identified using MS/MS and LC-MS/MS.

The identified proteins in Tables 1 and 2 have been annotated according to Gene Ontology (GO), including their predicted functions (Fig. 5). Six categories were created: metabolism, expression, structure, neuronal functions, signalling and defence, corresponding to major cellular and neuronal functions. The most diverse category was expression, with 34% identified proteins participating in transcription, splicing, translation, folding, transport and protein degradation; then in descending order of abundance proteins with neuronal functions (20%), metabolism (19%), signalling (13%), defence (8%) and finally structural proteins (6%). Structural proteins represented the most abundant proteins: vimentin (VIM), tubulins (Tbα and β) and actin (β-ac in figure 1a). This diversity was respected for proteins identified from photoreceptor cells (Fig. 2).

We next enlarged this study by comparing with data obtained from rodless *rd1* mouse retina (Fig. 1, right panel). Proteins involved in photoreceptor function, such as β-transducin (Tβ1 and 2), recoverin (Rec), 14.3.3 proteins (14ζ/α/ε), exhibit reduced level in the rodless retina as expected (fig. 1a). After rod degeneration a large increase in the content of the crystallin protein family was observed (αCM, m and αCb, βC2 and 3 in figure 1b). A low level of the α-crystallin A Major component (αCM) was also detected in the normal retina (Fig. 1a). The induction of α-crystallin B (αCb) expression was examined using western blotting (Fig. 6a). Expression was compared between wild type and *rd1* mice during and after rod degeneration, and only low levels of immunoreactivity were detected in wild type retina at both ages (lanes 1 and 2) as compared with the internal standard (Fig. 6b).

This qualitative analysis led to the identification of 212 spots by MALDI-TOF MS, nanoESI-MS/MS and LC-MS/MS, representing 109 different proteins.

Discussion :

This is to our knowledge the first proteomic study of mouse retina, with unambiguous identification of 212 spots. Only 27 spots (13%) did not give any information. The vast majority of the 2D gel features were identified by peptide mass fingerprinting combined with MALDI-TOF MS analysis. Only a small number of silent spots were resolved by MS/MS and peptide sequencing. Concerning unidentified features, several reasons could be proposed. First, an ineffective tryptic digestion may result in a low yield of peptide extraction from the gel, and hence impaired mass spectrometric analysis. Second, the extensive post-translational modifications could generate unpredictable peptide masses thus weakening the database search. Third, tryptic peptides outside the experimental mass range of 1000-4000 *m/z* will not be considered. Finally, the protein could be unknown and not yet included in the protein databases, and would thus require complete sequencing (Edman microsequencing or *de novo* MS/MS). The percentage coverage of identified proteins ranged from 6-86%. Several studies have demonstrated that validation of the identifications relies on several elements including random matches (32). In order to minimize false results, we took into account the correlation between the observed molecular weight of the protein (Fig. 1 and 2) and its identification (MW in Table 1).

The predicted locations of the proteins within cellular compartments represent the entire spectra, ie. nuclear (37%), mitochondrial (25%), endoplasmic (15%) and membrane proteins (15%). Nevertheless it should be noticed that rhodopsin was not found, while this 7 transmembrane receptor is very abundant in photoreceptors. Out of 5 integral membrane proteins identified, three [TACE, acetylglucosaminyl transferase (agt) and

metalloendopeptidase (Mep)] have only one transmembrane domain, and the other two (UCP2 and channel VdC) are multiple transmembrane domain proteins from mitochondrial membranes. The presence of the latter in our analysis may be a consequence of their specific subcellular location.

Figure 5 is a schematic view of the diversity of functions required for normal retinal physiology. It is not surprising that proteins participating in expression are represented in abundance since the retina, and more specifically the PR, have the highest metabolic rate in the body, for example constant renewal of disks (33). Six splicing factors that most probably correlate with their abundance in retina were recognised. Even if these proteins mediate some basic biological process with no tissue specificity, the finding of disease-causing mutations in splicing factors demonstrates their importance in retinal function (34-36). Analysis of the retinal proteome provides a new approach in the search for genes involved in retinal dystrophies. One detected major protein, Cyclophillin A (CyA), shares extensive homology to ninaA, a gene involved in photoreceptor degeneration in Drosophila (37-38). The cyclophillin A gene maps to the RP9 locus but no mutation mapping to that locus has been found in retinitis pigmentosa families (Shomi Bhattacharya, personal communication), consistent with the recent identification of Pim-1 gene mutations at that locus (39). Proteins involved in cell signalling were also identified (TACE, Ulip2, 4 and Prp). The importance of TNF-α Converting Enzyme is highlighted by its specific inhibition by the TIMP3 gene product, involved in macular degeneration (40-41). The proteins clustered in the category annotated defence include apoptosis, redox control and immune response (Fig. 5). The sustained protein synthesis in retinal tissues implies a large production of reactive oxygen products that are known to be neurotoxic (42-43). Two peroxyredoxins (Px2 and 5), enzymes involved in the reduction of these reactive products were identified. Thioredoxin, a protein

controlling redox potential, has been shown to prevent photoreceptor degeneration *in vitro* (44).

Using a differential approach, we found expression of crystallins from the small heat shock family (sHSP) (45-46) to be greatly increased after rod degeneration. A link between α-crystallin B induction and rod degeneration is suggested by our analysis by western blotting (Fig. 5) and by previous studies (47). The level of α-crystallin B was found to be elevated at both ages examined, with a maximum at 15 days postnatal (PN), the stage of maximal rod degeneration in the *rd1* mouse (5). The mechanism of sHSP regulation involves an increase in steady state levels of their mRNA, as observed using micro-array analysis (data not shown). Upregulation of α-crystallin B has been observed in many stress-inducing conditions, from oxidative stress to Alzheimer disease (46, 48). In addition, it is a specific constituent of drusen in patients suffering from aged-related macular degeneration (49).This observation has been extented by providing evidence that other members of the crystallin family are also highly upregulated. The two proteins α-B and α-A constitute subunits of a multimeric complex that functions as a chaperone. α-crystallin B has been shown to block apoptosis induced by many stimuli (50). This activity is mediated by preventing the activation of the proenzyme caspase 3 (51) or alternatively by preventing the aggregation of the tau protein (52) with mutated proteins carrying a polyglutamine track (53). It is not known if the formation of a functional complex containing various sHSP is necessary for inhibition of apoptosis. The presence of crystallin proteins after all rods have degenerated suggests that the protein is not produced exclusively by rods, but most likely by surrounding cells such as Müller glial cells in response to signals triggered by rod apoptosis (54). It is paradoxical that rod apoptosis induces the expression of an anti-apoptotic protein in surrounding cells. The increase in crystallin family protein content in cells that do not express the mutated protein (PDE6B) responsible for the disease might constitute a general

mechanism, since it has been observed in many pathological conditions (46). This pathway might provide alternative targets for the development of neuroprotective therapies in this model.

Acknowledgments :

This work was financed by Inserm, Université Louis Pasteur, the Fondation de l'Avenir, the Association Française contre la Myopathie (AFM), Retina France, Ipsen foundation, Novartis and the European Community (PRO-AGE-RET program). The authors thank Donald Zack and David Hicks for critical reading of the manuscript.

References :

1. Farber, D. B. (1995). *Invest. Ophthalmol. Vis. Sci*. **36**, 261-275

2. Lolley, R. N., Farber, D. B., Rayborn, M. E., and Hollyfield, J. G. (1977). *Science*. **196**, 664-666.

3. Chang, G., Q., Hao, Y., and Wong, F. (1993). *Neuron*. **11**, 595-605

4. Portera-Cailliau, C., Sung, C. H., Nathans, J., and Adler, R. (1994). *Proc. Natl. Acad. Sci. U S A*. **91**, 974-978

5. Carter-Dawson, L. D., LaVail, M. M., and Sidman, R. L. (1978). *Invest. Ophthalmol. Vis. Sci.* 17, 489-498

6. Mohand-Said, S., Deudon-Combe, A., Hicks, D., Simonutti, M., Forster, V., Fintz, A. C., Leveillard, T., Dreyfus, H., and Sahel, J. A. (1998). *Proc. Natl. Acad. Sci. U S A*. **95**, 8357-8362

7. Fintz, A. C., Audo, I., Hicks, D., Léveillard, T., and Sahel, J. A. *Invest. Ophthalmol. Vis. Sci*. **44**, 818-825

8. Guillonneau, X., Piriev, N. I., Danciger, M., Kozak, C. A., Cideciyan, A. V., Jacobson, S. G., and Farber, D. B. (1999). *Hum. Mol. Genet.* **8**, 1541-1546

9. Kennan, A., Aherne, A., Palfi, A., Humphries, M., McKee, A., Stitt, A., Simpson, D. A., Demtroder, K., Orntoft, T., Ayuso, C., Kenna, P. F., Farrar, G. J., Humphries, P. (2002). *Hum. Mol. Genet*. **11**, 547-557

10 Livesey, F. J., Furukawa, T., Steffen, M. A., Church, G. M., Cepko, C. L. **(**2000). *Curr. Biol*. **23**, 301-310

11. Farjo, R., Yu, J., Othman, M. I., Yoshida, S., Sheth, S., Glaser, T., Baehr, W., Swaroop, A. (2002). *Vision Res*. **42**, 463-470

12 Blackshaw, S., Fraioli, R. E., Furukawa, T., Cepko, C. L. (2001). *Cell.* **107**, 579-589

13. Gygi, S. P., Rochon, Y., Franza, B. R., Aebersold, R. (1999). *Mol. Cell. Biol.* **19**, 1720-1730

14. Henzel, W. J., Billeci, T. M., Stults, J. T., Wong, S. C., Grimley, C., and Watanabe, C. (1993). *Proc. Natl. Acad. Sci. U S A*. **90**, 5011-5015

15. Mann, M., Hojrup, P., and Roepstorff, P. (1993). *Biol. Mass Spectrom.* **22**, 338-345

16. James, P., Quadroni, M., Carafoli, E., and Gonnet, G. (1993). *Biochem. Biophys. Res. Commun.* **195**, 58-64

17. Yates, J. R. 3rd., Speicher, S. , Griffin, P. R., Hunkapiller, T. (1993). *Anal. Biochem*. **214**, 397-408

18. Wilm, M., Shevchenko, A., Houthaeve, T., Breit, S., Schweigerer, L., Fotsis, T., and Mann, M. (1996). *Nature*. **379**, 466-469

19. Shevchenko, A., Wilm, M., Vorm, O., and Mann, M. (1996). *Anal. Chem*. **68**, 850-858

20. Shevchenko, A., Chernushevich, I., Wilm, M., and Mann, M. (2000). *Methods Mol. Biol.* **146**, 1-16

21. Mc Cormack, A. L. Schieltz, D. M., Goode, B. Yang, S., Barnes, G., Drubin, D., and Yates, J. R. (1997). *Anal. Chem*. **69**, 767-776

22. Rabilloud, T., Strub, J.-M., Luche, S., Van Dorsselaer, A., and Lunardi, J. (2001). *Proteomics*. **1**, 699-704

23. Scheler, C., Lamer, S., Pan, Z., Li, X. P., Salnikow, J., and Jungblut, P. (1998). *Electrophoresis*. **19**, 918-927

24. Fontaine, V., Kinkl, N., Sahel, J. A., Dreyfus, H., and Hicks, D. (1998). *J. Neurosci.* **18**, 9662-9672

25. Jensen, O. N., Podtelejnikov, A., and Mann, M. (1996). *Rapid Commun. Mass Spectrom*. **10**, 1371-1378

26. Rudd, P. M., Colominas, C., Royle, L., Murphy, N., Hart, E., Merry, A. H., Hebestreit, H. F., and Dwek, R. A. (2001). *Proteomics*. **1**, 285-294

27. Rabilloud, T. (1996). *Electrophoresis*. **17**, 813-829

28. Krause, E., Wenschuh, H., and Jungblut, P. R. (1999). *Anal. Chem*. **71**, 4160-4165

29. de Hoffmann, E. (1996). *J. Mass Spectrom*. **31**, 129-137

30. Stevens, S. M. Jr., Kem, W. R., and Prokai., L. (2002). *Rapid Commun. Mass Spectrom*. **16**, 2094-2101

31. Roepstorff, P., and Fohlman, J. (1984). *Biomed. Mass Spectrom.* **11**, 601-615

32. Eriksson, J. and Fenyö, D. (2002). A model of random mass-matching and its use for automated significance testing in mass spectrometric proteome analysis. *Proteomics*. **2**, 262-270

33. La Cour, M. (2003). The retinal pigment epithelium. In *Physiology of the eye* (P. L. Kaufman, A. Alm, Ed.), pp. 348-357

34. Vithana, E. N, Abu-Safieh, L., Allen, M. J., Carey, A., Papaioannou, M., Chakarova, C., Al-Maghtheh, M., Ebenezer, N. D., Willis, C., Moore, A. T., Bird, A. C., Hunt, D. M., and Bhattacharya, S. S. (2001). *Mol. Cell*. **8**, 375-381

35. McKie, A. B., McHale, J. C., Keen, T. J., Tarttelin, E. E., Goliath, R., van Lith-Verhoeven, J. J., Greenberg, J., Ramesar. R. S., Hoyng, C. B., Cremers, F. P., Mackey, D. A., Bhattacharya, S. S., Bird, A. C., Markham, A. F., Inglehearn, C. F. (2001). *Hum. Mol. Genet*. **10**, 1555-1562

36. Chakarova, C. F., Hims, M., M., Bolz, H., Abu-Safieh, L., Patel, R. J., Papaioannou, M. G., Inglehearn, C. F., Keen, T. J., Willis, C., Moore, A. T., Rosenberg, T., Webster, A. R., Bird, A. C., Gal, A., Hunt, D., Vithana, E. N., and Bhattacharya, S. S. (2002). *Hum. Mol. Genet.* **11**, 87-92

37. Schneuwly, S., Shortridge, R. D., Larrivee, D. C., Ono, T., Ozaki, M., Pak, W. L. (1989). *Proc. Natl. Acad. Sci. U S A.* **86**, 5390-5394

38. Ferreira, P. A., Hom, J. T., and Pak, W. L. (1995). *J. Biol. Chem*. **270**, 23179-23188

39. Keen, T. J., Hims, M. M., McKie, A. B., Moore, A. T., Doran, R. M., Mackey, D. A., Mansfield, D. C., Mueller, R. F., Bhattacharya, S. S., Bird, A. C., Markham, A. F., and Inglehearn, C. F. (2002). *Eur. J. Hum. Genet*. **10**, 245-249

40. Amour, A., Slocombe, P. M., Webster, A., Butler, M., Knight, C. G., Smith, B. J., Stephens, P. E., Shelley, C., Hutton, M., Knauper, V., Docherty, A. J., and Murphy, G. (1998). *FEBS Lett.* **435**, 39-44

41. Weber, B. H., Vogt, G., Pruett, R. C., Stohr, H., and Felbor, U. (1994). *Nat. Genet.* **8**, 352-356

42. Winkler, B. S., Boulton, M. E., Gottsch, J. D., and Sternberg, P. (1999). *Mol. Vision*. **5**, 32-42

43. Picaud S., (2003). Retinal biochemistry. In *Physiology of the eye* (P. L. Kaufman, A. Alm, Ed.), pp. 382-408

44. Tanito, M., Masutani, H., Nakamura, H., Ohira, A., and Yodoi, J. (2002). *Invest. Ophthalmol. Vis. Sci.* **43**, 1162-1167

45. Muchowski, P. J., Hays, L. G., Yates, J. R. 3rd, and Clark, J. I. (1999). *J. Biol. Chem*. **274**, 30190-30195

46. van Rijk, A. F., and Bloemendal, H. (2000). *Ophthalmologica*. **214**, 7-12

47. Jones, S. E., Jomary, C., Grist, J., Thomas, M. R., and Neal, M. J. (1998). *Neuroreport*. **9**, 4161-4165

48. Rogalla, T., Ehrnsperger, M., Preville, X., Kotlyarov, A., Lutsch, G., Ducasse, C., Paul, C., Wieske, M., Arrigo, A. P., Buchner, J., and Gaestel, M. (1999). *J. Biol. Chem* . **274**, 18947-18956

49. Crabb, J. W., Miyagi, M., Gu, X., Shadrach, K., West, K. A., Sakaguchi, H., Kamei, M., Hasan, A., Yan, L., Rayborn, M. E., Salomon, R. G., and Hollyfield, J. G. (2002). *Proc. Natl. Acad. Sci. U S A.* **99**, 14682-14687

50. Mehlen, P., Schulze-Osthoff, K., and Arrigo, A. P. (1996). *J. Biol. Chem.* **271**, 16510-16514

51. Kamradt, M. C., Chen, F., and Cryns, V. L. (2001). *J. Biol. Chem*. **276**, 16059-16063

52. Dou, F., Netzer, W. J., Tanemura, K., Li, F., Hartl, F. U., Takashima, A., Gouras, G. K., Greengard, P., and Xu, H. (2003). *Proc. Natl. Acad. Sci. U S A*. **100**, 721-726

53. Cummings, C. J., Sun, Y., Opal, P., Antalffy, B., Mestril, R., Orr, H. T., Dillmann, W. H., and Zoghbi, H. Y. (2001). *Hum. Mol. Genet.* **10**, 1511-1518

54. Iwaki, T., Wisniewski, T., Iwaki, A., Corbin, E., Tomokane, N., Tateishi, J., and Goldman, J. E. (1992). *Am. J. Pathol.* **140**, 345-356

Figure legends :

Figure 1: 2D gel electrophoresis separation of neural retina extracts after coomassie staining. Left panel: wild type mouse retina; right panel: *rd1* mouse retina. Annotations according to Table 1.

Figure 2: 2D gel electrophoresis separation of photoreceptors extracted from wild type mouse retina isolated by vibratome sectioning.

Figure 3: MALDI-TOF MS spectrum obtained after treatment of a spot by trypsin digestion. Peptides from □: pyruvate kinase; ◇: phosphoglycerate mutase; ○: creatine kinase; Δ : phosphoglycerate kinase.

Figure 4 : nano-ESI MS/MS spectra obtained after isolation and fragmentation. a: ion $(M+2H)^{2+}$ at *m/z* 513.35; b: ion $(M+2H)^{2+}$ at *m/z* 488.32 ; c: ion $(M+2H)^{2+}$ at *m/z* 542.92. The interpreted amino acid sequences are depicted at the top of each spectrum. The spectra were treated by deconvolution before database searching.

Figure 5 : Schematic view of functions performed by the identified proteins. Italic letters correspond to annotation from Gene Ontology. The percentage of broader categories are indicated at the center of the graph.

Figure 6 : Western blotting analysis. Lanes 1 and 2: wild type; 3 and 4 *rd1*. Lanes 1 and 3: 15 days postnatal; 2 and 4 : 35 days postnatal. a, α-crystallin B ; b, α-tubulin.

Table 1 : List of identified proteins by MALDI-TOF MS and their annotations.

Spot N°	Protein	Abb.	Coverage %	Accession N°	MW Calculated (kDa)	Predicted function	Gene ontology
A1	Lumican	LUM	18%	P51885	38.3	Extracellular Matrix	GO : 0005578
A2	Splicing factor 3a1	SF3	6%	NP_080451	75.7	Splicing	
A5	RAB-23 (open brain)	R23	21%	P35288	26.7	Transport	GO : 0006886
A6	Hsp110	h110	13%	Q61316	94.1	Chaperone	GO : 0003773
A8	Tumor rejection Antigen	TRA	35%	P08113	92.5	Chaperone	GO : 0003754
A11	Lamin B1	LB1	62%	P14733	66.9	Cytoskeleton	GO : 0005882
A12	Hnrpk	Hnrp	24%	Q60577	51.0	Splicing	GO : 0030529
A14	Vimentin	Vim	82%	P20152	53.7	Cytoskeleton	GO : 0005882
A15	Tubulin α–1	Tbα	59%	P02551	50.1	Cytoskeleton	GO : 0007018
A17	ATP synthase β	ATPβ	51%	P56480	56.6	Energetic metabolism	GO : 0006754
A19	Enolase 1	Eno	60%	P17182	47.1	Glycolysis	GO : 0006096
A22	β-actin	βac	61%	P02570	41.7	Cytoskeleton	GO : 0005200
A23	Creatin kinase brain	Cki	55%	Q04447	42.7	Glycolysis	GO : 0004111
A24-26	Transducin β1	Tβ1	41%	P04901	37.3	Vision	
	Transducin β2	Tβ2	22%	P54312	37.3	Vision	
A31	Peroxiredoxin 2	Px2	71%	Q61171	21.8	Redox	GO : 0016209
A32	PE-binding protein	Peb	30%	P70296	20.9	Signal transduction	
A33	Histone h2b f	H2b	51%	P10853	13.9	Transcription	GO : 0005718
A35	β-synuclein	βSy	35%	Q16143	14.3	Synaptic transmission	
A37	Cytochrome c oxidase	Cyc	13%	P12787	16.2	Energetic metabolism	GO : 0006118
A42	Recoverin	Rec	51%	P34057	23.4	Vision	GO : 0007601
A43	14-3-3 protein ζ	14ζ	53%	P35215	27.7	Vision	
	14-3-3 protein α	14α	27%	P31946	27.7	Vision	
A44	Phosphoglycerate mutase	PgM	74%	P18669	28.8	Glycolysis	GO : 0006096
A47	EF1α1	Eα1	22%	P10126	50.1	Translation	GO : 0003746
	EF1α2	Eα2	21%	P27706	50.1	Translation	GO : 0003746
A49	PTB-splicing factor	PTB	27%	P23246	76.1	Splicing	GO : 0006371
A55	Glutamine synthase	GlS	44%	P15105	42.1	Glutamate metabolism	GO : 0004356
A62	LDH-A	LDH	56%	P06151	36.8	Glycolysis	GO : 0006096
A67	Cyclophilin A	CyA	55%	P17742	17.9	Chaperone	GO : 0006457
A68	Ubiquitin	Ubn	72%	P02248	8.6	Protein degradation	
A69	Vacuolar ATPase	vATP	31%	P50516	68.2	Energetic metabolism	GO : 0006754
A70	Calretinin	CaR	16%	Q08331	31.4	Ca^{2+}-binding	GO : 0005509
A71	S-arrestin	Arr	47%	P20443	44.9	Vision	GO : 0007601
A73	Histone H2A.3	H2a	67%	P20671	14.1	Transcription	GO : 0005718
A74	Chromatin assembly factor	CAF	11%	Q13112	61.0	Transcription	GO : 0005634
A76	P 450 11B2	P450	8%	P15539	57.0	Steroid hormone biosynthesis	GO : 0006700
A78	Transaminase	Trm	23%	P05202	47.4	Glutamate metabolism	GO : 0006520
	Acetyl-CoA acetyltransferase	Act	12%	P24752	45.2	Glycolysis	GO : 0003985
A79	Hypothetical cytochrom c fam.	ZnF	12%	BAB28569	42.9	Transcription	GO : 0005634
	CDK9	CDK9	14%	NP_570930	42.7	Transcription	
A80	60S protein ribosomal	60S	17%	P40429	23.6	Translation	GO : 0003735
	40S ribosomal protein S3A	40S	19%	P97351	30.0	Translation	GO : 0006412
A81	snRNP	Snrp	14%	P43331	13.9	Splicing	GO : 0006371
	T-box transcription factor	Tbx	13%	P70325	19.8	Transcription	GO : 0003700
A96	Hsp 94		24%	P48722	94.3	Chaperone	
A104	Vesicular fusion P		20%	P46460	82.5	Transport	GO : 0008565
A105	Actin interacting protein		38%	O88342	66.4	Cytoskeleton	GO : 0005856
A106	Ulip 2		34%	O08553	62.1	Cell Signalling	
A109	Unc-18 homolog		18%	O08599	67.7	Transport	GO : 0008565
A113	Ulip 4		30%	O35098	61.9	Cell Signalling	
A116	TACE		13%	Q9Z0F8	73.8	Cell Signalling	
A117	Dihydrolipoamide deshydrogenase		21%	O08749	54.2	Energetic metabolism	GO : 0006118

Table 1 : Continued

Spot N°	Protein	Abb.	Coverage %	Accession N°	MW calculated (kDa)	Predicted function	Gene ontology
A134	Fructose bisphosphate aldolase		63%	P05064	39.2	Glycolysis	GO : 0006096
	Oligo synthetase		33%	P11928	42.4	Immune response	GO : 0006955
A138	HnRNP A2		29%	O88569	36.0	Splicing	GO : 0030529
A139	Mitochondrial malate deshydrogenase		35%	P08249	35.6	Glycolysis	GO : 0006099
A140	Capping β		25%	P47757	30.6	Cytoskeleton	GO : 0005200
A146	UCP 2		20%	P70406	33.4	Energetic metabolism	GO : 0006839
A150	RAN		34%	P17080	24.4	Transport	GO : 0008565
	RGS 18		21%	Q99PG4	27.6	Signal transduction	GO : 0007165
	BAD		17%	Q61337	22.1	Apoptosis	GO : 0006915
A151	Triose P isomerase		55%	P17751	26.6	Glycolysis	GO : 0006096
A155	Phospholipase A2 IIF		27%	Q9QZT4	18.9	Signal transduction	
A157	Lactoylglutathione lyase		35%	Q9CPU0	20.7	Redox	
	Phosphatidylinositol transfert P		22%	P53810	31.7	Signal transduction	GO : 0004462
B1	α crystallin A, major component	αCM	86%	P02490	19.4	Chaperone	
B2	α crystallin A, minor component	αCm	43%	P24622	22.5	Chaperone	
B6	β crystallin B3	βC3	60%	Q9JJU9	24.3	Chaperone	
B29	Fus	Fus	14%	P56959	52.7	Splicing	GO : 0003723
B31	Carbonic anhydrase	CAII	54%	P00920	29.0	Glycolysis	GO : 0004089
B33	GDP dissociation Inhibitor 1	GDI	29%	P50936	36.6	Transport	
B36	α crystallin B chain	αCB	21%	P23927	20.1	Chaperone	
B39	Peroxiredoxin 5	Px5	40%	O08709	24.9	Redox	GO : 0016209
	Triose P isomerase	TPI	30%	P17751	26.7	Glycolysis	GO : 0006096
B42	β crystallin B2	βC2	40%	P26775	23.4	Chaperone	
C6	Tubulin β-5 chain	Tbβ	37%	P05218	49.7	Cytoskeleton	GO : 0005198
C25	Voltage-dependent anion channel 1	VdC	41%	Q60932	36.5	Apoptosis	GO : 0008308
C33	ISGF-3G	I3G	14%	Q61179	44.6	Transcription	GO : 0003700
C42	Calreticulin	CaN	48%	P14211	48.0	Ca^{2+}-binding	GO : 0005514
C43	Valosin containing Protein	VCP	43%	Q01853	89.3	Transport	GO : 0006810
	Metalloendopeptidase	Mep	10%	P70669	86.4	Protein degradation	GO : 0006508
C45	Hsp86-1 α	H86α	45%	P07901	84.8	Chaperone	GO : 0003773
	Hsp86-1 β	H86β	28%	P11499	83.3	Chaperone	GO : 0003773
C46	Hspa5	ha5	55%	P20029	72.4	Chaperone	
C48	Hspa8	ha8	46%	P08109	70.9	Chaperone	GO : 0003773
	Hsp70.1	h70	24%	P17879	70.0	Chaperone	GO : 0003773
C49	PDI	PDI	47%	P09103	57.1	Redox	
C50	Phosducin	Pho	61%	Q9QW08	28.0	Vision	GO : 0007601
	Proliferin related protein	Prp	21%	P04769	27.9	Cell signalling	GO : 0005179
C51	14-3-3 protein ε	14ε	70%	P42655	29.2	Vision	
C53	HMG-1	HMG	51%	P07155	24.9	Transcription	GO : 0006355
C54	K-ras	ras	22%	P32883	21.7	Signal transduction	GO : 0007264
C56	GAPDH	Gdh	74%	P16858	35.8	Glycolysis	GO : 0006096
C58	Acetyl glucosaminyl transferase	agt	18%	P97402	45.5	Extracellular matrix	
C63	Cytoplasmic malate deshydrogenase	Mdh	47%	P14152	36.5	Glycolysis	GO : 0006899
C65	Glutamate oxaloacetate transaminase 1	Got	39%	P05201	46.2	Glutamate metabolism	GO : 0006520
	Aldolase 3C	Ald	33%	P05063	25.0	Glycolysis	GO : 0006096
C67	Phosphoglycerate kinase	PhK	56%	P09411	44.5	Glycolysis	GO : 0006096
	Mitonchondrial creatin kinase	CKm	38%	P30275	47.0	Glycolysis	GO : 0004111
C69	Glutamate deshydrogenase	Gld	10%	P26443	61.3	Glutamate metabolism	GO : 0004353
C70	ATP synthase α	ATPα	31%	Q03265	59.8	Energetic metabolism	GO : 0006754

Table 2 : Identification from MS/MS and LCMS/MS analysis

Spots	**Analysis**	**Precursor ion (charge)**	**Fragment ions ***	**Identified sequence**	**Identified protein**	**Accession N°**	**MW calculated**	**Predicted Function**	**Gene Ontology**
A45	MS/MS	640.3 (2+)	$y_{10},y_9,y_8,y_7,y_2,y_1$	GEHPGXXXAK	HMG-1	P09429	24.9	Transcription	GO : 0006365
A50	MS/MS	611.3 (2+)	y_4,y_3,y_2,y_1	VLTK	Pyruvate kinase	P52480	57.9	Glycolysis	GO : 0006096
		586.0 (2+)	b_1,b_2,b_3,b_4,b_5,b_6	LDIDSA					
C13	MS/MS	564.4 (1+)	y_3,y_2,y_{31}	FELR	ATF-2	P16951	42.0	Transcription	GO : 0006365
A77	LCMS/MS	513.4 (2+)	$y_9,y_8,y_7,y_6,y_5,y_4,y_2,y_1$	IGGIGTVPVGR				Translation	GO : 0003746
		488.3 (2+)	$y_7,y_6,y_5,y_4,y_3,y_2,y_1$	LPLQDVYK	EF-1α	P34823	49.3		
A83	LCMS/MS	542.9 (2+)	$y_{10},y_9,y_8,y_7,y_6,y_5,y_4,y_3,y_2,y_1$	GSPLVVISQGK	Ulip2	O08553	62.1	Cell signalling	
B46	LCMS/MS	898.0 (2+)	$y_9,y_6,y_4,y_1/\ b_7,b_8,b_9$	MLSDGRTIITFPNG TR	Tcp-10	S26413	49.5	Immune response	
B47	LCMS/MS	713.9 (2+)	$y_{10},y_9,y_8\ ,y_7,y_6,y_4,y_2,/b_2\ ,b_6$	VTVYELENFQGK	β crystallin B3	Q9JJU9	24.3	Chaperone	

* ion fragments are labelled according to the nomenclature of Roepstorff (1984). y and b fragments correspond to rupture of the peptidic bond with charge carried on the C and N terminus respectively. The accompanying number corresponds to the position of the amino acid in the sequence.

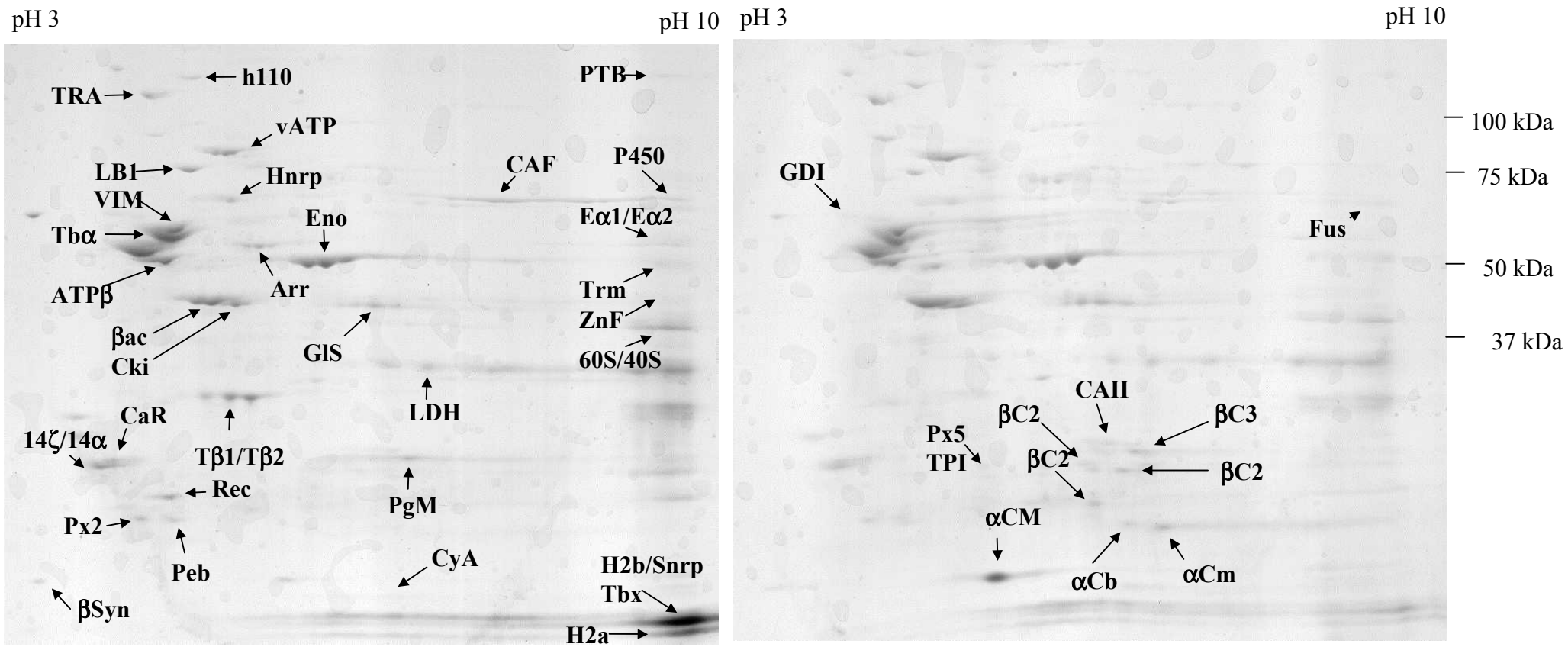
pH 3
pH 10
h110
TRA
PTB
vATP
LB1
Hnrp
CAF
P450
VIM
Eno
Eα1/Eα2
Tbα
ATPβ
Arr
Trm
ZnF
βac
Cki
GlS
60S/40S
LDH
CaR
14ζ/14α
Tβ1/Tβ2
Rec
PgM
Px2
Peb
CyA
H2b/Snrp
Tbx
βSyn
H2a
pH 3
pH 10
100 kDa
75 kDa
50 kDa
37 kDa
GDI
Fus
CAII
βC2
βC3
Px5
TPI
βC2
βC2
αCM
αCb
αCm

Figure 1

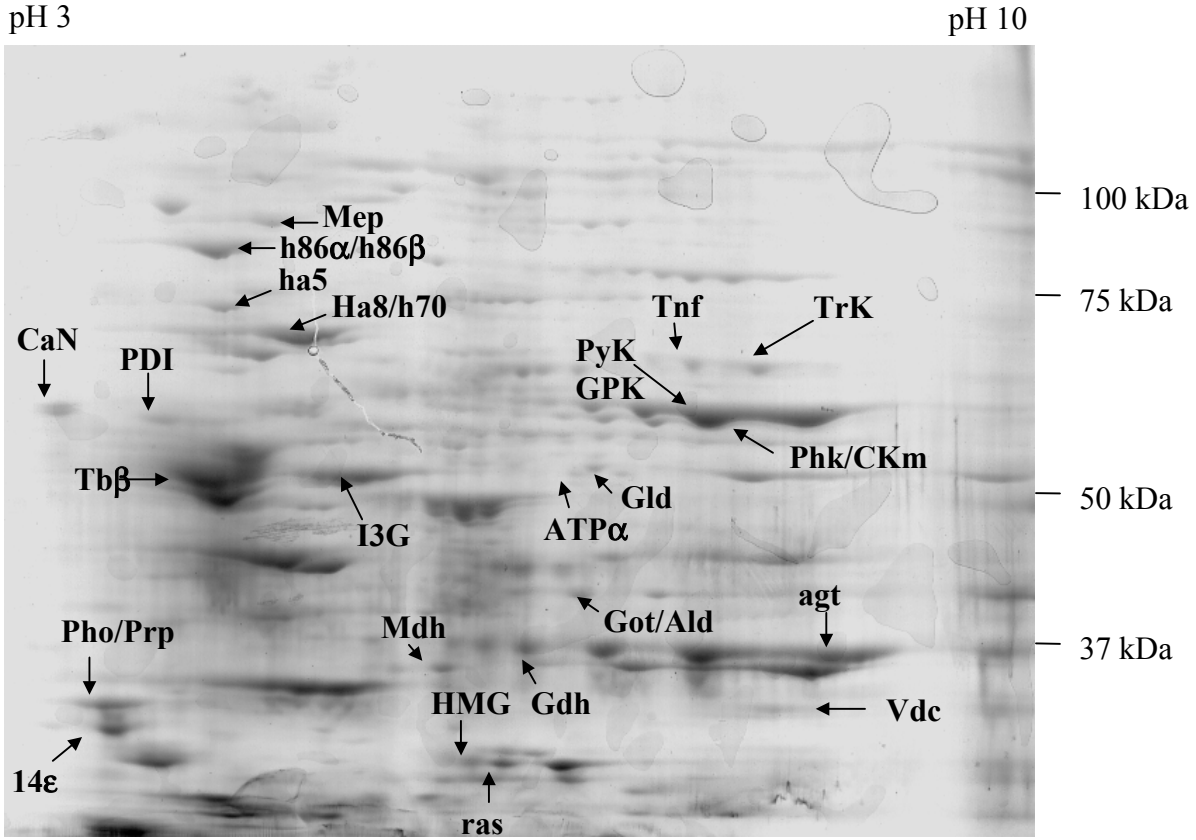
pH 3
pH 10
100 kDa
75 kDa
50 kDa
37 kDa
Mep
h86α/h86β
ha5
Ha8/h70
CaN
PDI
Tnf
TrK
PyK
GPK
Phk/CKm
Tbβ
I3G
Gld
ATPα
agt
Got/Ald
Pho/Prp
Mdh
HMG
Gdh
Vdc
14ε
ras

Figure 2

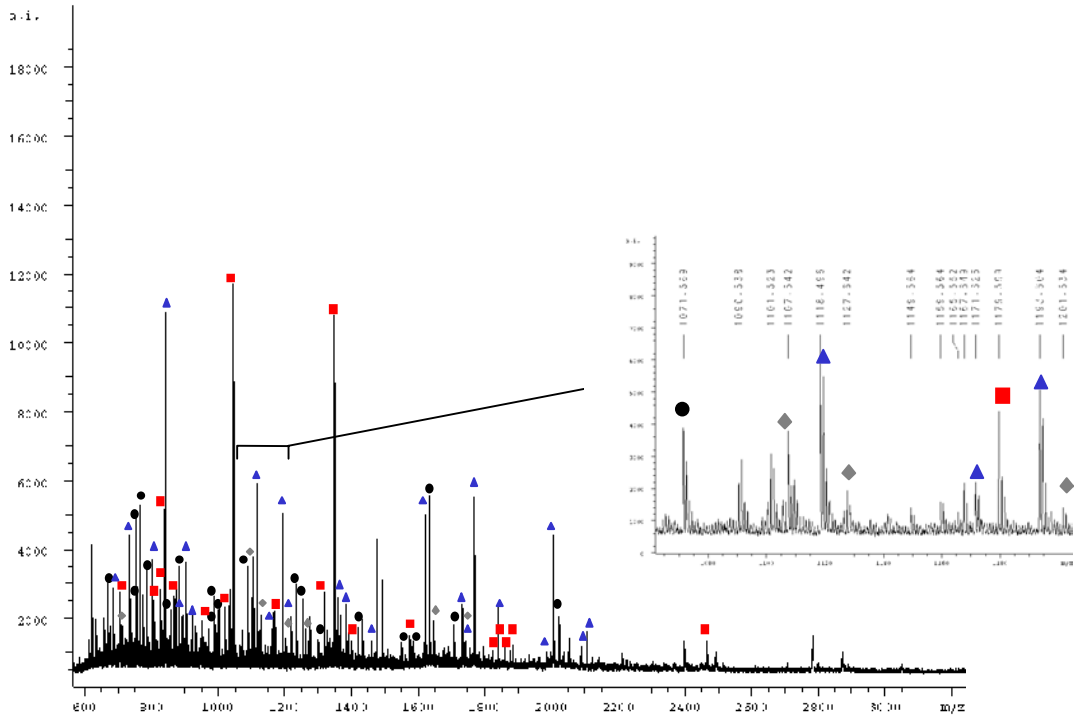

Figure 3

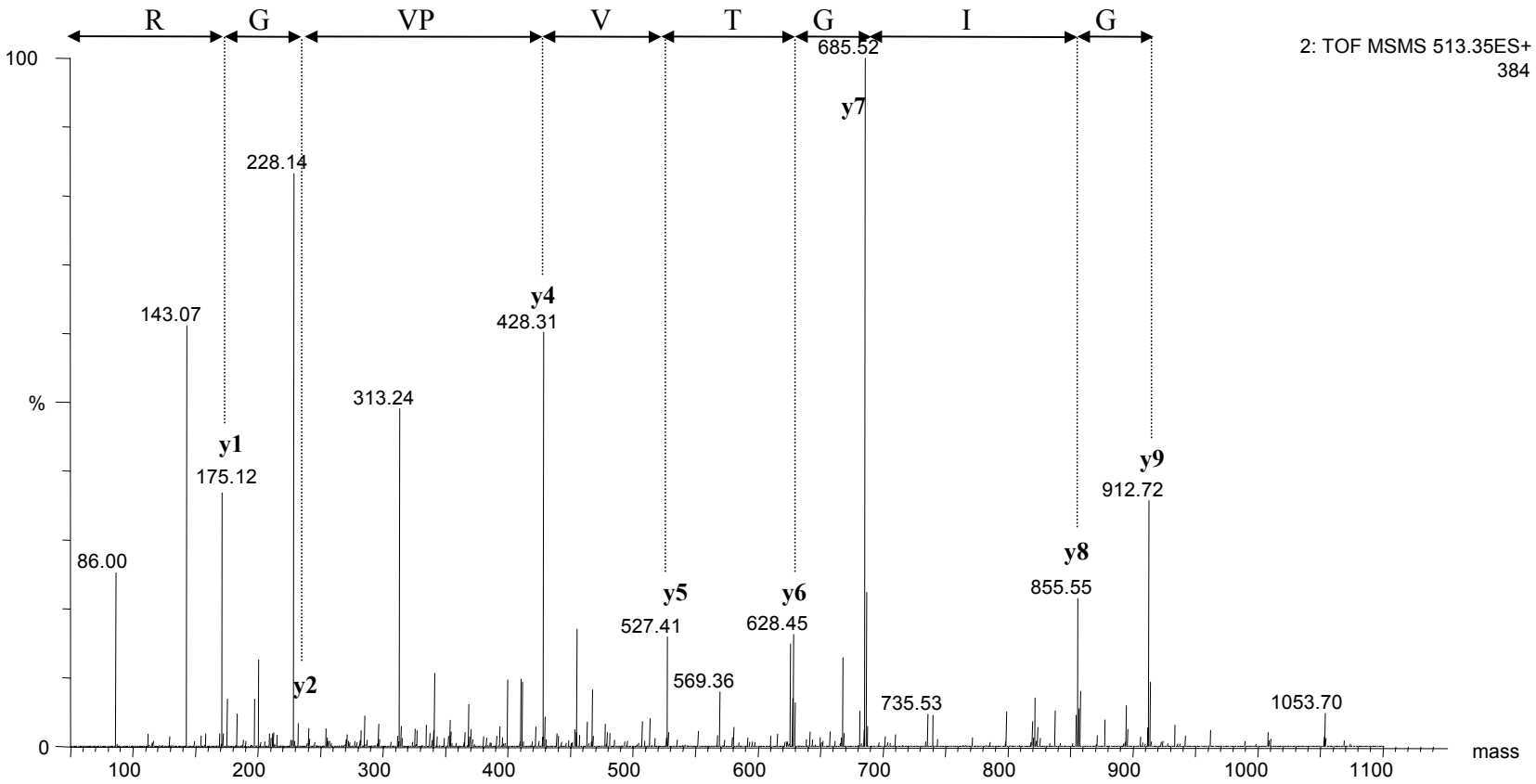
R
G
VP
V
T
G
I
G
2: TOF MSMS 513.35ES+
384
100
%
0
685.52
y7
228.14
y4
428.31
143.07
313.24
y1
175.12
y9
912.72
86.00
y8
855.55
y5
527.41
y6
628.45
y2
569.36
735.53
1053.70
100
200
300
400
500
600
700
800
900
1000
1100
mass

Figure 4a

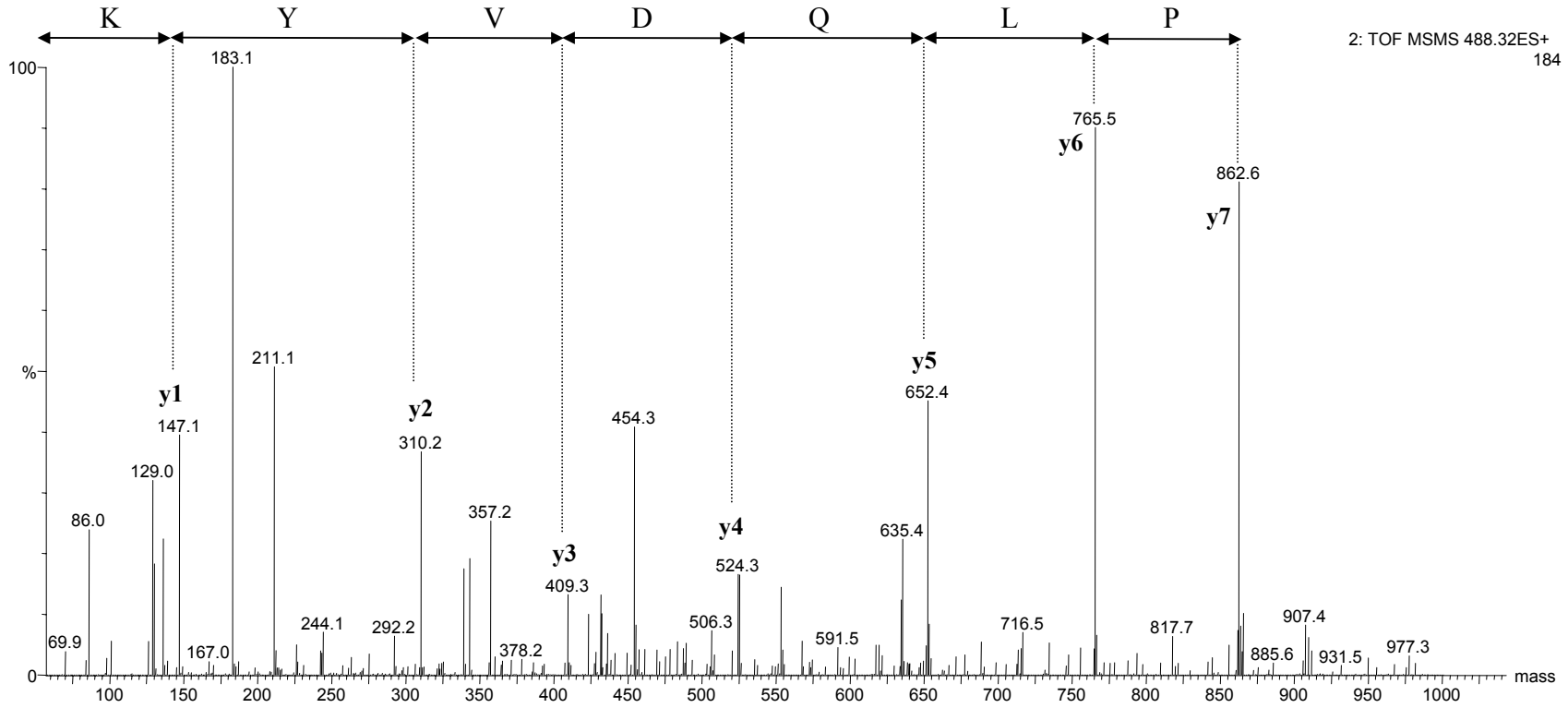
K
Y
V
D
Q
L
P
2: TOF MSMS 488.32ES+
184
100
%
0
183.1
765.5
y6
862.6
y7
211.1
y5
652.4
y1
147.1
y2
310.2
454.3
129.0
86.0
357.2
y4
524.3
635.4
y3
409.3
69.9
167.0
244.1
292.2
378.2
506.3
591.5
716.5
817.7
907.4
885.6
931.5
977.3
mass
100
150
200
250
300
350
400
450
500
550
600
650
700
750
800
850
900
950
1000

Figure 4b

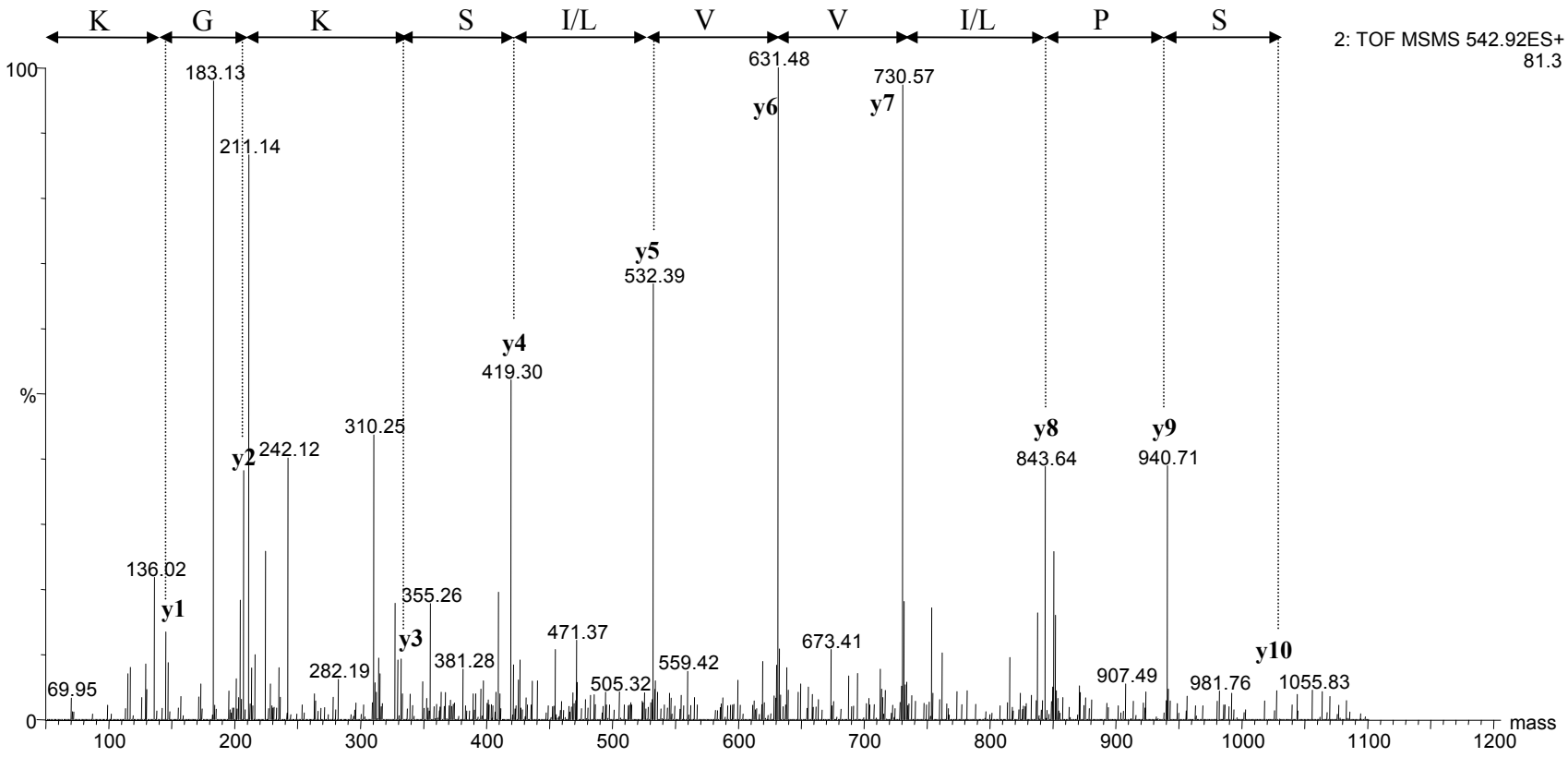
K G K S I/L V V I/L P S
2: TOF MSMS 542.92ES+
81.3
100
%
0
mass
100 200 300 400 500 600 700 800 900 1000 1100 1200
183.13
211.14
631.48
y6
730.57
y7
y5
532.39
y4
419.30
310.25
242.12
y2
y8
843.64
y9
940.71
136.02
y1
355.26
y3
471.37
673.41
y10
282.19
381.28
559.42
907.49
981.76
1055.83
505.32
69.95

Figure 4 c

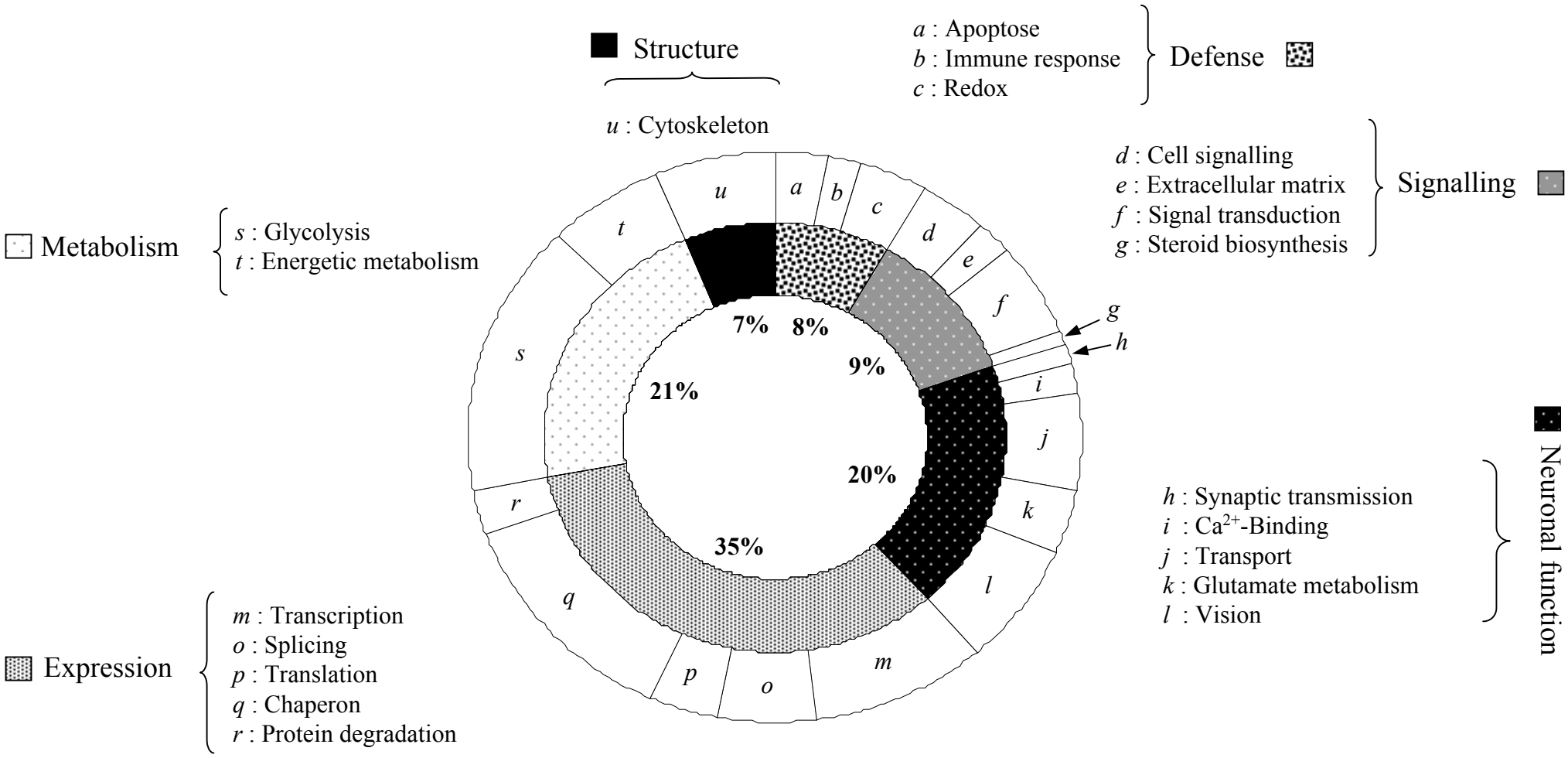
Structure
u : Cytoskeleton
a : Apoptose
b : Immune response
c : Redox
Defense
d : Cell signalling
e : Extracellular matrix
f : Signal transduction
g : Steroid biosynthesis
Signalling
Metabolism
s : Glycolysis
t : Energetic metabolism
7%
8%
9%
21%
20%
35%
h : Synaptic transmission
i : Ca2+-Binding
j : Transport
k : Glutamate metabolism
l : Vision
Neuronal function
Expression
m : Transcription
o : Splicing
p : Translation
q : Chaperon
r : Protein degradation

Figure 5

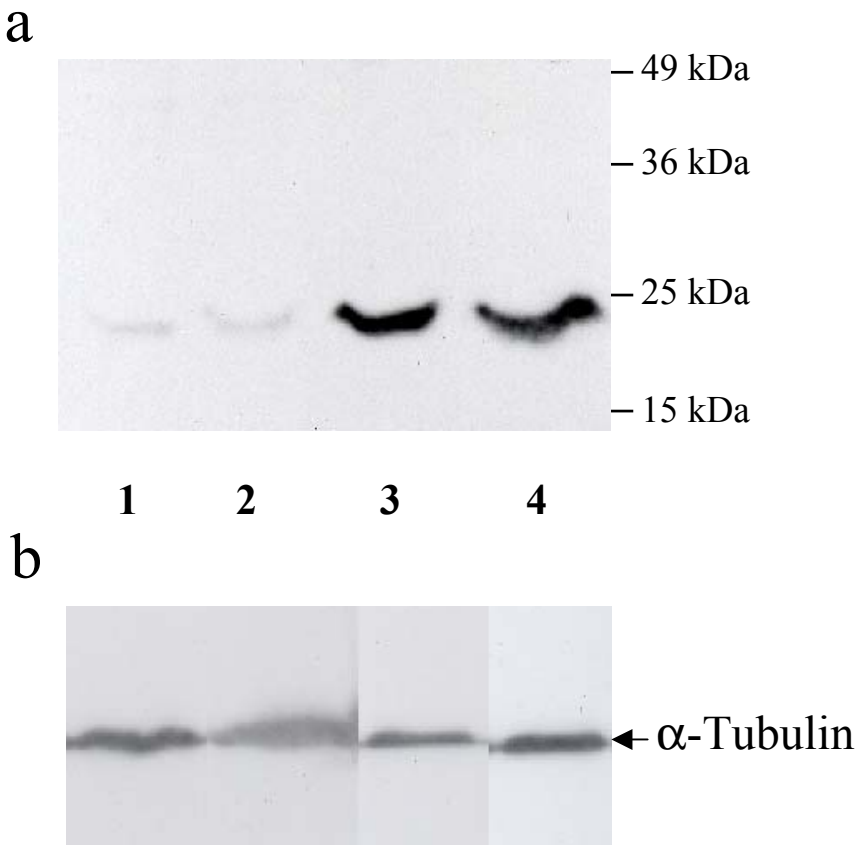

Figure 6